Models and parameters							
Model	**Description**	$R_{\textbf{crit}}$ **[m]**	D_c **[m]**	μ_d	γ	**Rigidity (dynamic relaxation simulation)**	**Rigidity (Dynamic rupture)**
Gaussian SDM							
1	Low rigidity model with negative shear stresses and very high P_f	3400	1.0	0.1	0.97	low	low
2	low rigidity model with non-negative shear stress changes and very high P_f	3400	1.0	0.1	0.97	low	low
3	Same setting as model 2 with slip-neutral friction zone replaced by slip-weakening friction	3400	1.0	0.1	0.97	low	low
4	Same setting as model 2 with slip-neutral and slip-strengthening friction zones replaced by slip-weakening friction	3400	1.0	0.1	0.97	low	low
5	High rigidity model and very high P_f	3400	1.0	0.1	0.97	high	high
6	Constant rigidity model and very high P_f	3400	1.0	0.1	0.97	constant	low
7	Model to assess the dynamic effect of the low rigidity	3400	1.0	0.1	0.97	high	low
8	Mixed P_f; γ = 0.62 when z < 10 km and γ = 0.97 when z > 10 km	3400	1.0	0.1	mixed	low	low
9	Low rigidity model with very high but slightly lower P_f	3400	1.0	0.1	0.96	low	low
10	Reference SFs x 2 and high P_f	1400	1.0	0.1	0.91	low	low
11	Reference SFs x 2 and high P_f	1400	1.0	0.1	0.88	low	low
12	Reference SFs x 2 and high P_f	1400	1.0	0.1	0.85	low	low
13	Reference SFs x 4 and moderate-high P_f	1200	1.0	0.1	0.71	low	low
14	Reference SFs x 4 and moderate-high P_f	1200	1.0	0.1	0.68	low	low
15	Reference SFs x 4 and moderate-high P_f	1200	1.0	0.1	0.65	low	low
16	Margin-wide rupture with higher scaling factor at center Oregon and very high P_f	4400	1.0	0.1	0.97	low	low
17	Southern epicenter and very high P_f	3400	1.0	0.1	0.97	low	low
18	Shallower coupling depth of 22 km and very high P_f	3400	1.0	0.1	0.97	low	low
shallow-coupled SDMs							
19	Negative shear stress rate tapered up to 30 km and very high P_f	7600	1.0	0.3	0.97	low	low
20	Negative shear stress rate tapered up to 30 km with smaller D_c and very high P_f	5400	0.7	0.3	0.97	low	low
21	Negative shear stress rate tapered up to 30 km with constant rigidity and very high P_f	5400	0.7	0.3	0.97	constant	low
22	Negative shear stress rate tapered up to 80 km and very high P_f	6200	0.7	0.3	0.98	low	low

Table S1: Parameters of the 3D dynamic rupture scenarios (model 1–22) investigated in this study. The scenarios are divided into two groups based on the underlying assumed SDM. Models 1–18 in the upper part of the Table use the Gaussian SDM of Schmalzle et al. (2014) and models 19–22 in the lower part use the shallow-coupled SDMs of Lindsey et al. (2021). 'Rigidity (dynamic relaxation simulation)' and 'Rigidity (Dynamic rupture)' labeled columns refer to the rigidity profiles we used for the dynamic relaxation simulations and the dynamic rupture simulations, respectively.

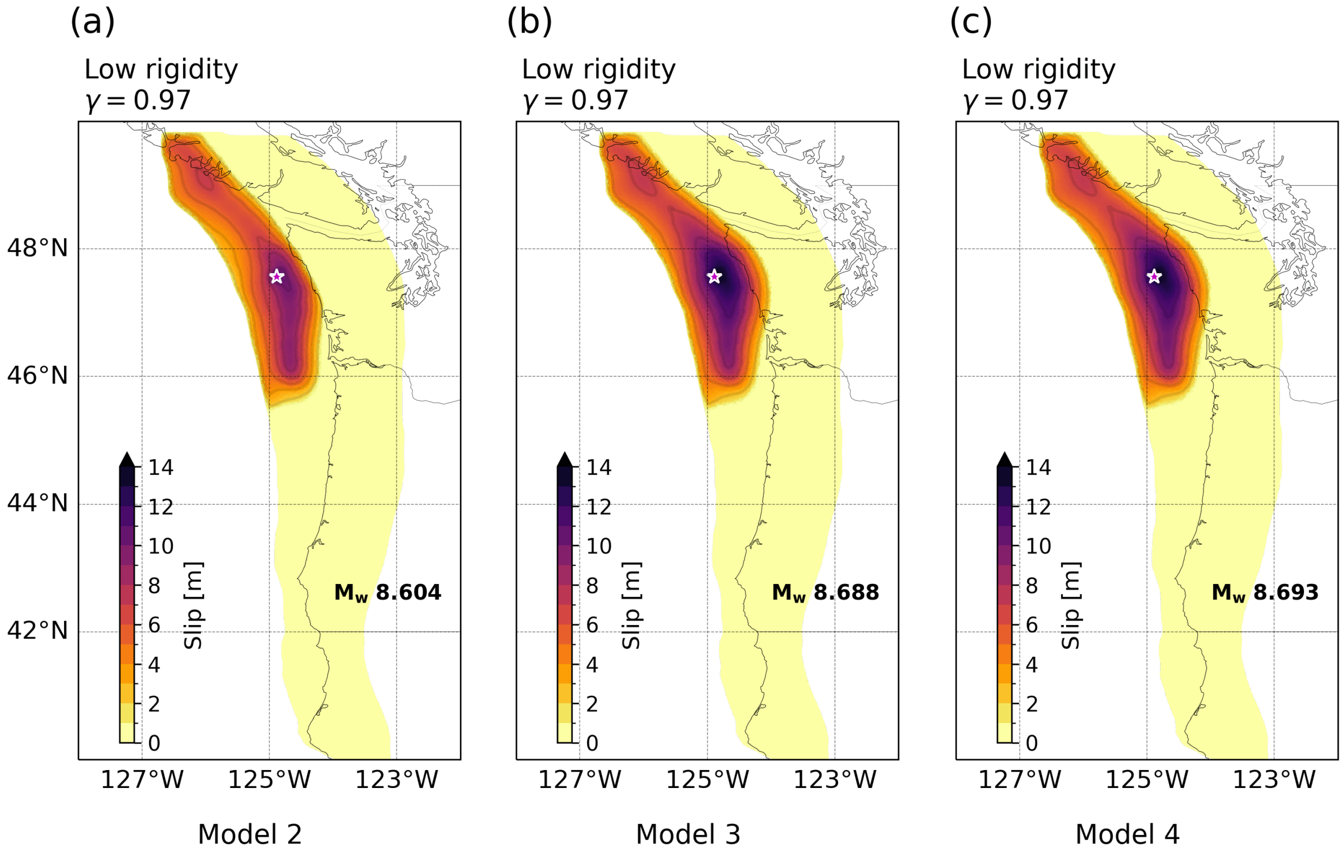

Figure S1: Effects of assuming slip-strengthening versus slip-neutral linear slip-weakening friction beneath the seismogenic zone (at depths >27 km), using a Gaussian SDM, low rigidity, and very high P_f where $\gamma = 0.97$. (a) Modeled fault slip for the dynamic rupture scenario (model 2) with slip-neutral ($\mu_d = \mu_s$) and slip-strengthening ($\mu_d > \mu_s$) friction below the seismogenic zone. (b) Modeled fault slip for the dynamic rupture scenario (model 3) with a sharp transition from slip-weakening to slip-strengthening regime with no slip-neutral zone. (c) Modeled fault slip for the dynamic rupture scenario (model 4) with linear slip-weakening friction parameterization everywhere and no slip-strengthening or slip-neutral frictional behavior. The magenta star denotes the rupture initiation location.

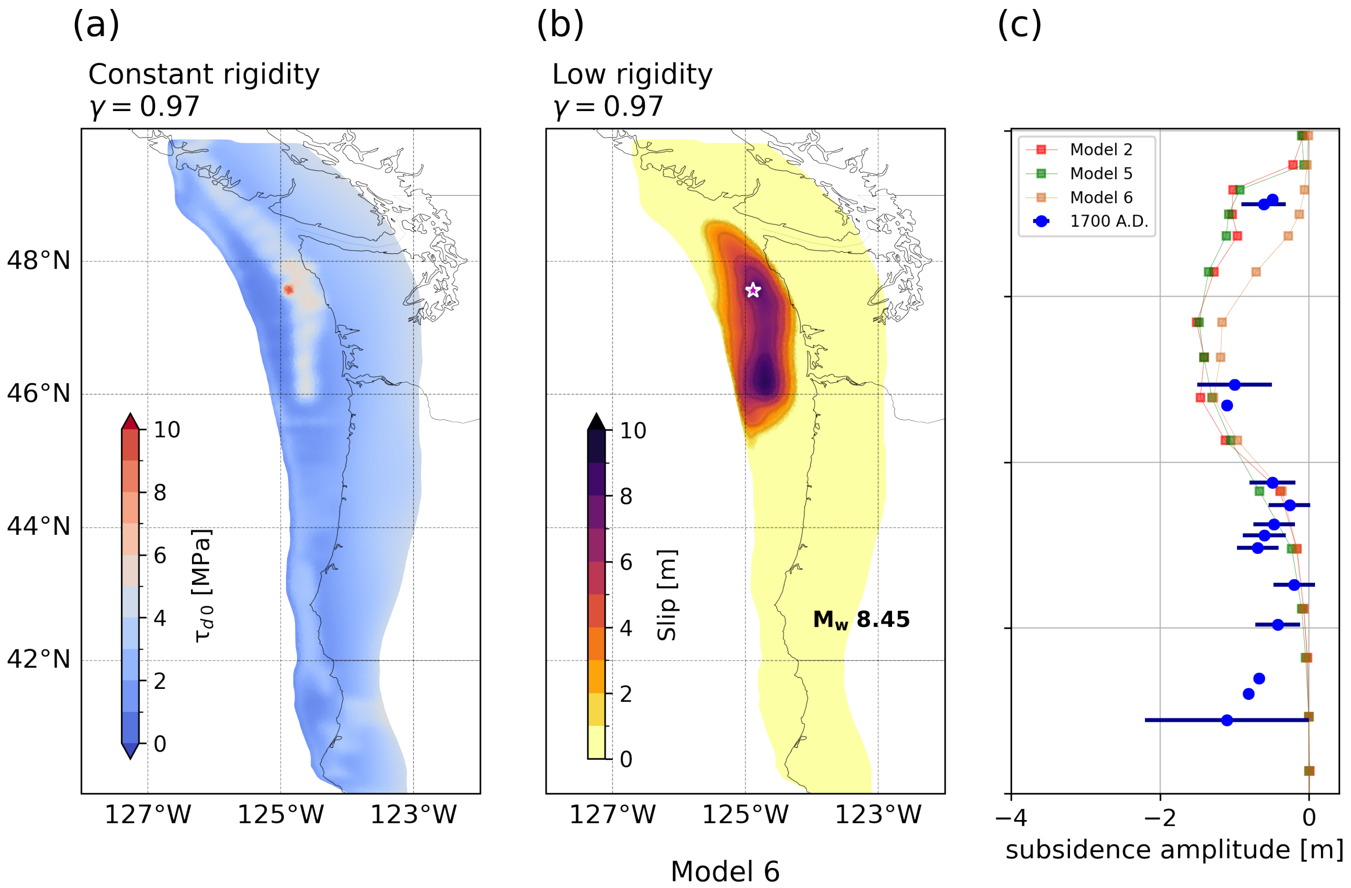

Figure S2: (a) Initial along-dip shear stresses and (b) Modeled slip for a dynamic rupture scenario (model 6) with constant rigidity used to calculate the initial stresses and a low rigidity in the dynamic rupture simulation, using a Gaussian SDM and very high P_f ratio ($\gamma = 0.97$). (C) Modeled subsidence (squares) for the constant rigidity rupture scenario (Chocolate), low rigidity rupture scenario (green, model 5), and high rigidity rupture scenario (red, model 5) and paleoseismic observations of the rupture of 1700 A.D. (Wang et al., 2013) (blue circles). The magenta star denotes the rupture initiation location (hypocenter).

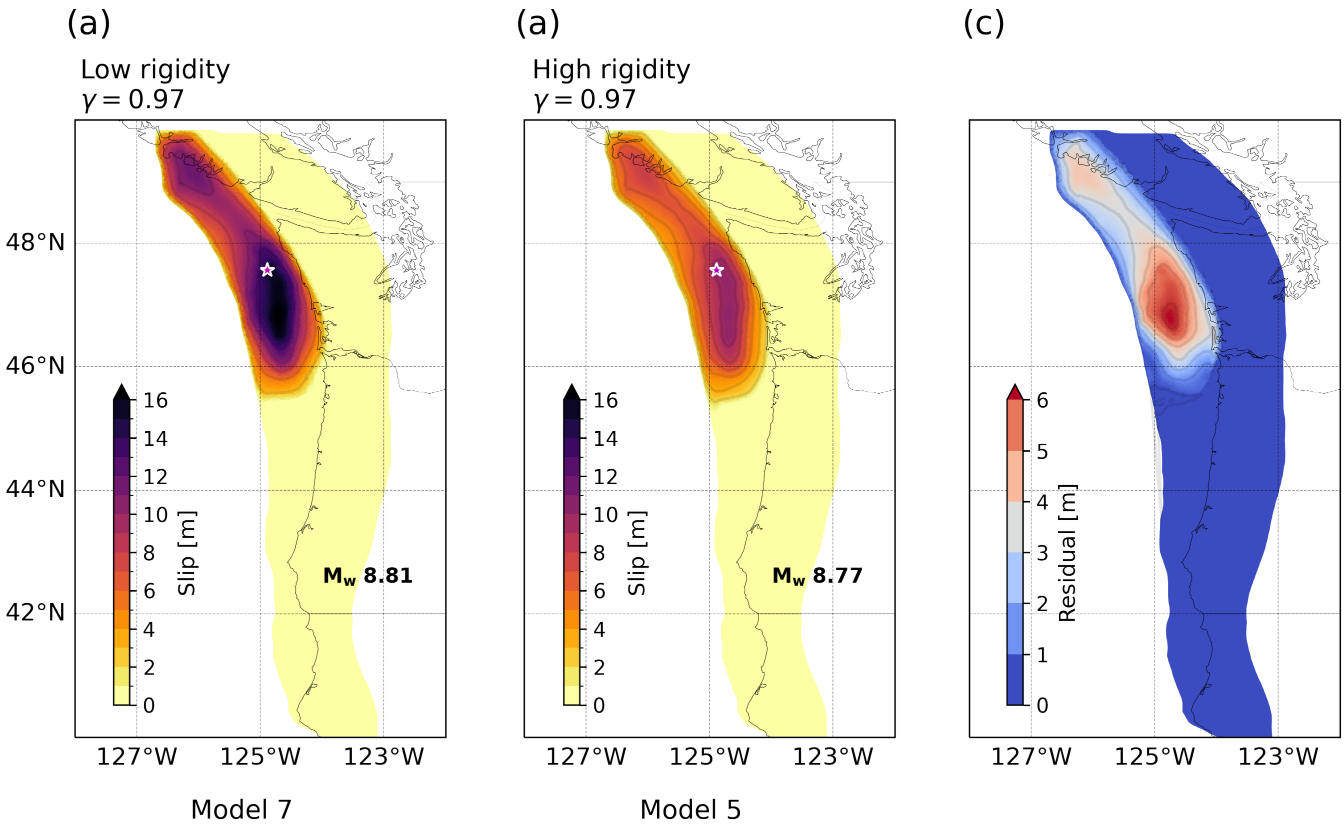

Figure S3: (a) The effect of using low rigidity (model 7) over (b) high rigidity (model 5) in dynamic rupture simulations. Both models use a Gaussian SDM with the initial stresses computed using high rigidity and very high P_f where $\gamma = 0.97$. (c) Difference in fault slip between the low- and the high-rigidity models (model 7 - model 5). The magenta star denotes the hypocenter where ruptures are initiated.

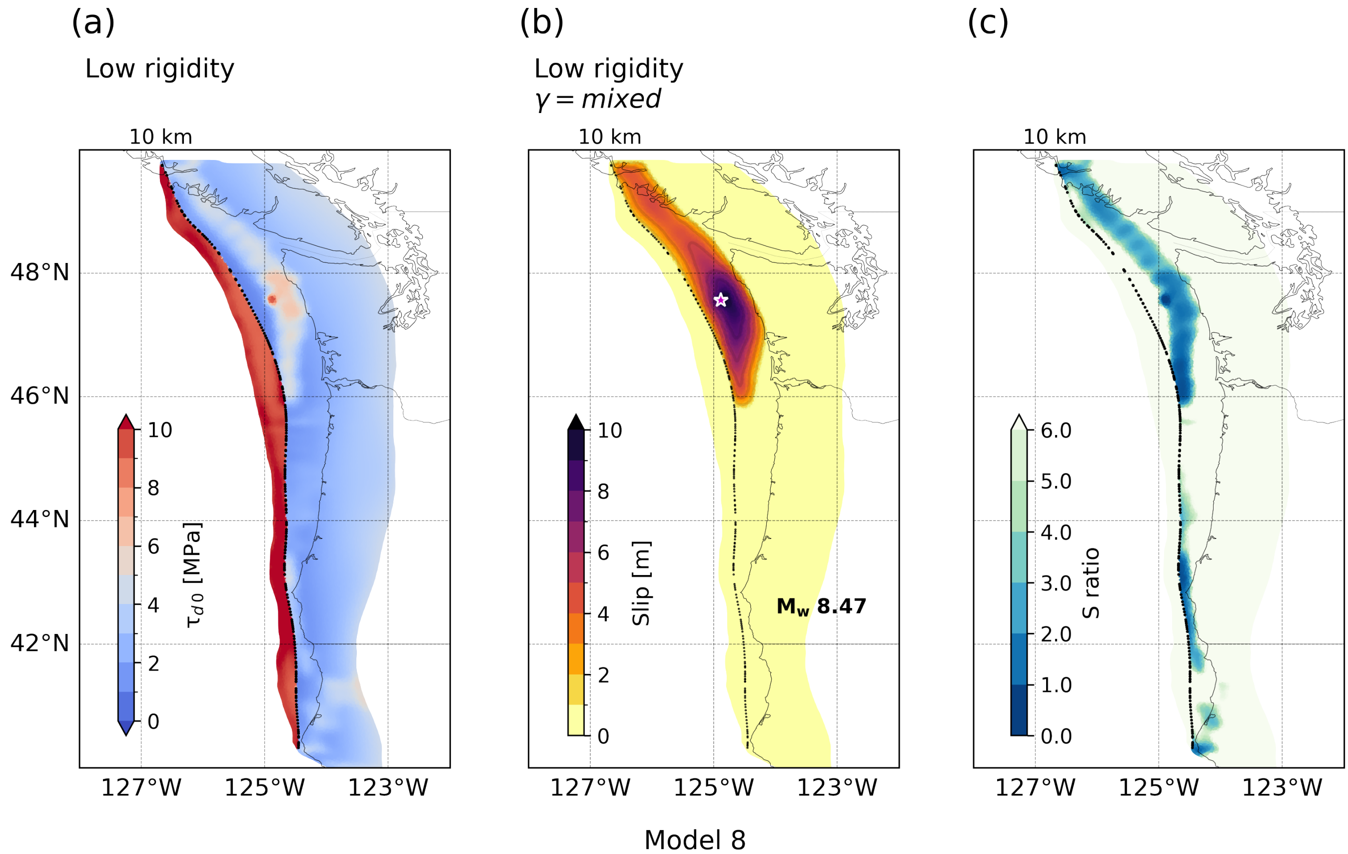

Figure S4: (a) Initial along-dip shear stresses and (b) modeled fault slip for a dynamic rupture scenario (model 8) with mixed P_f ratio. Moderate P_f ratio ($\gamma = 0.62$) at depth < 10 km and very high P_f ratio ($\gamma = 0.97$) at depth > 10 km, using a Gaussian SDM and low rigidity. (C) The S ratio for this scenario reaches almost zero close to the trench. Black dashed lines denote the 10 km depth contour. The magenta star denotes the rupture initiation location (hypocenter).

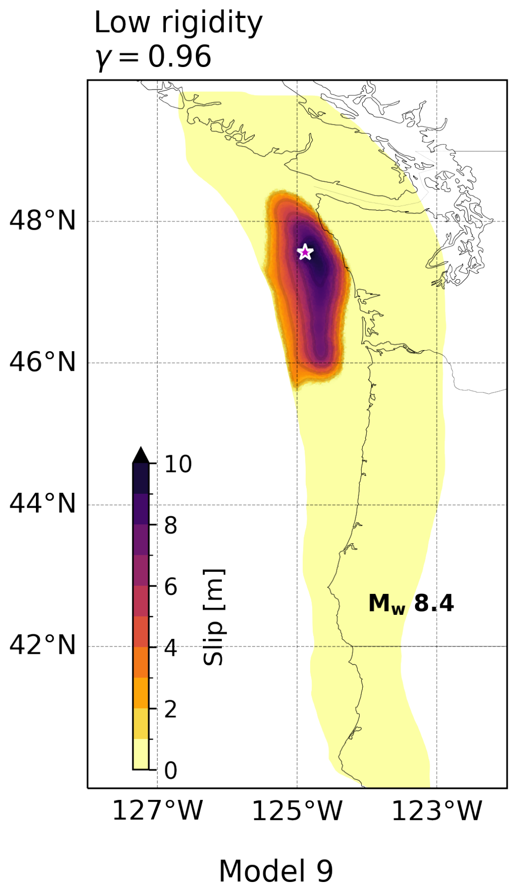

Figure S5: Modeled fault slip of the dynamic rupture scenario (model 9) with very high P_f ratio (γ=0.96), using a Gaussian SDM and low rigidity. The magenta star denotes the rupture initiation location (hypocenter).

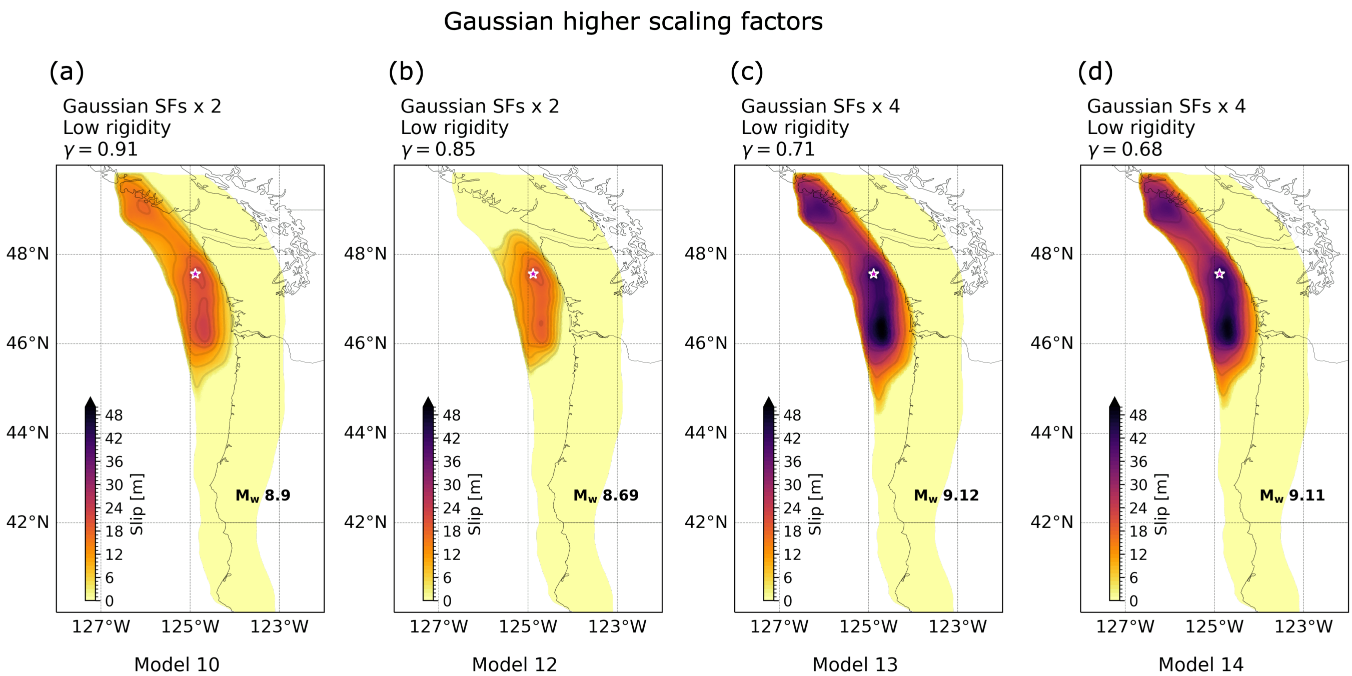

Figure S6: Modeled fault slip of the dynamic rupture scenarios (models 10, 12, 13, and 14) with slip deficit calculated using the reference scaling factors (SFs): times 2 (a) and (b) and times 4: (c) and (d) and different levels of P_f ratio using a Gaussian SDM and low rigidity. The magenta star denotes the rupture initiation location (hypocenter).

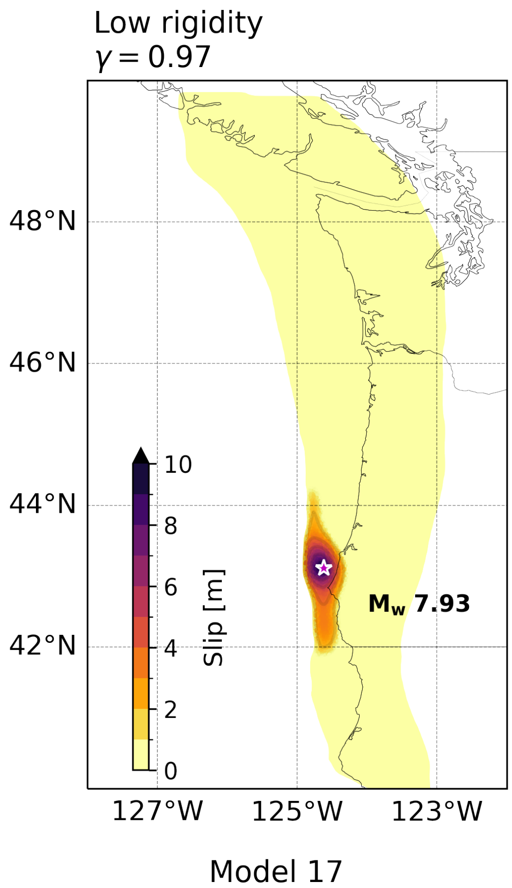

Figure S7: Modeled fault slip of the dynamic rupture scenario (model 17) with a southern epicenter, using a Gaussian SDM, low rigidity, and very high P_f ratio ($\gamma = 0.97$). The magenta star denotes the rupture initiation location (hypocenter).

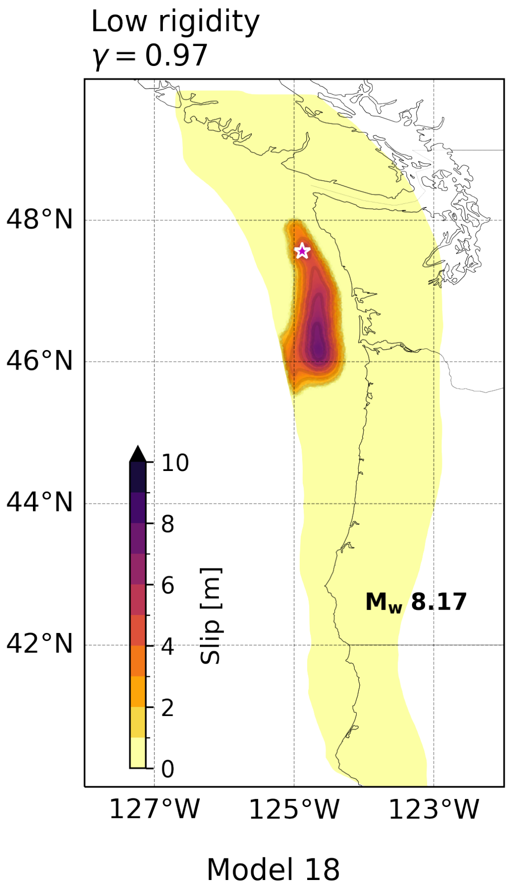

Figure S8: Modeled fault slip of the dynamic rupture scenario (model 18) with a shallow coupling depth of 22 km (compared to 27 km in all the other models) using a Gaussian SDM, low rigidity, and very high P_f ratio ($\gamma = 0.97$). The magenta star denotes the rupture initiation location (hypocenter).

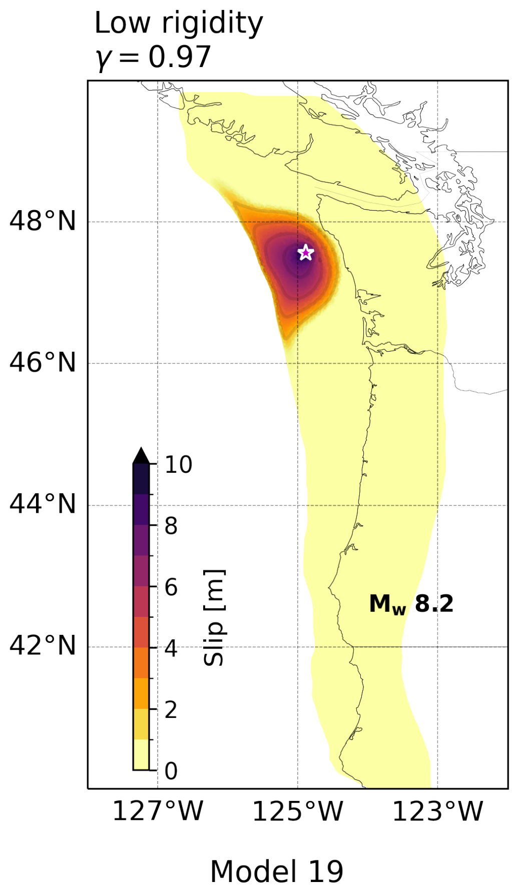

Figure S9: Modeled fault slip of the dynamic rupture scenario (model 19) with low rigidity and very high P_f ratio ($\gamma = 0.97$) using the shallow-coupled 30 SDM, with D_c=1 m. The magenta star denotes the hypocenter where rupture is initiated.

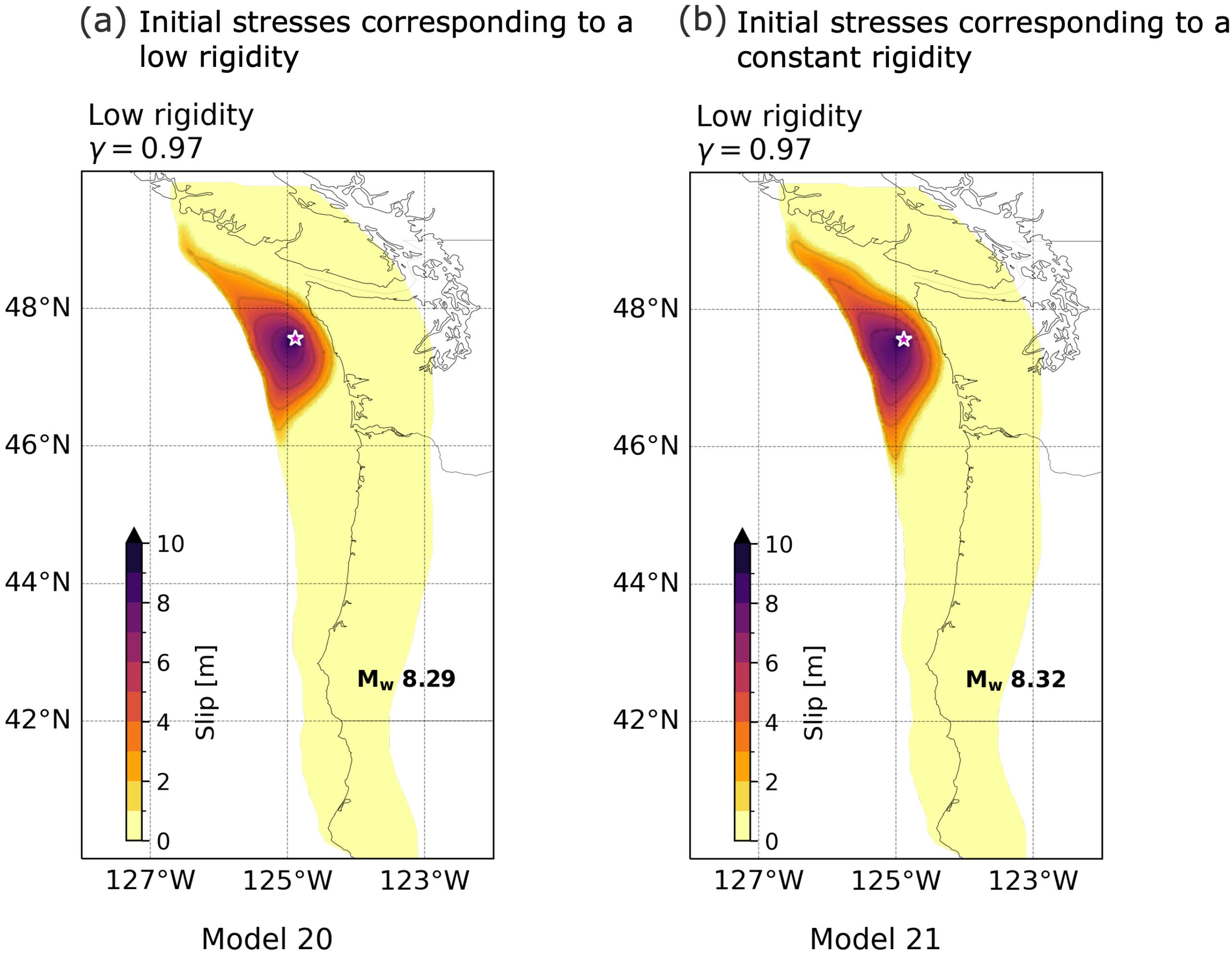

Figure S10: (a) Modeled fault slip of the dynamic rupture scenario (model 20) with shallow-coupled 30 SDM and a low rigidity used in the dynamic relaxation and the dynamic rupture simulations. (b) Modeled fault slip of the dynamic rupture scenario (model 21) with shallow-coupled 30 SDM and a constant rigidity of 32 GPa used in the dynamic relaxation simulation but a low rigidity for a dynamic rupture simulation. All other parameters are similar to model 20; we use a very high P_f ratio of $\gamma = 0.97$, low rigidity profile during the dynamic rupture simulation and D_c of 0.7 m. The magenta star denotes the rupture initiation location (hypocenter).

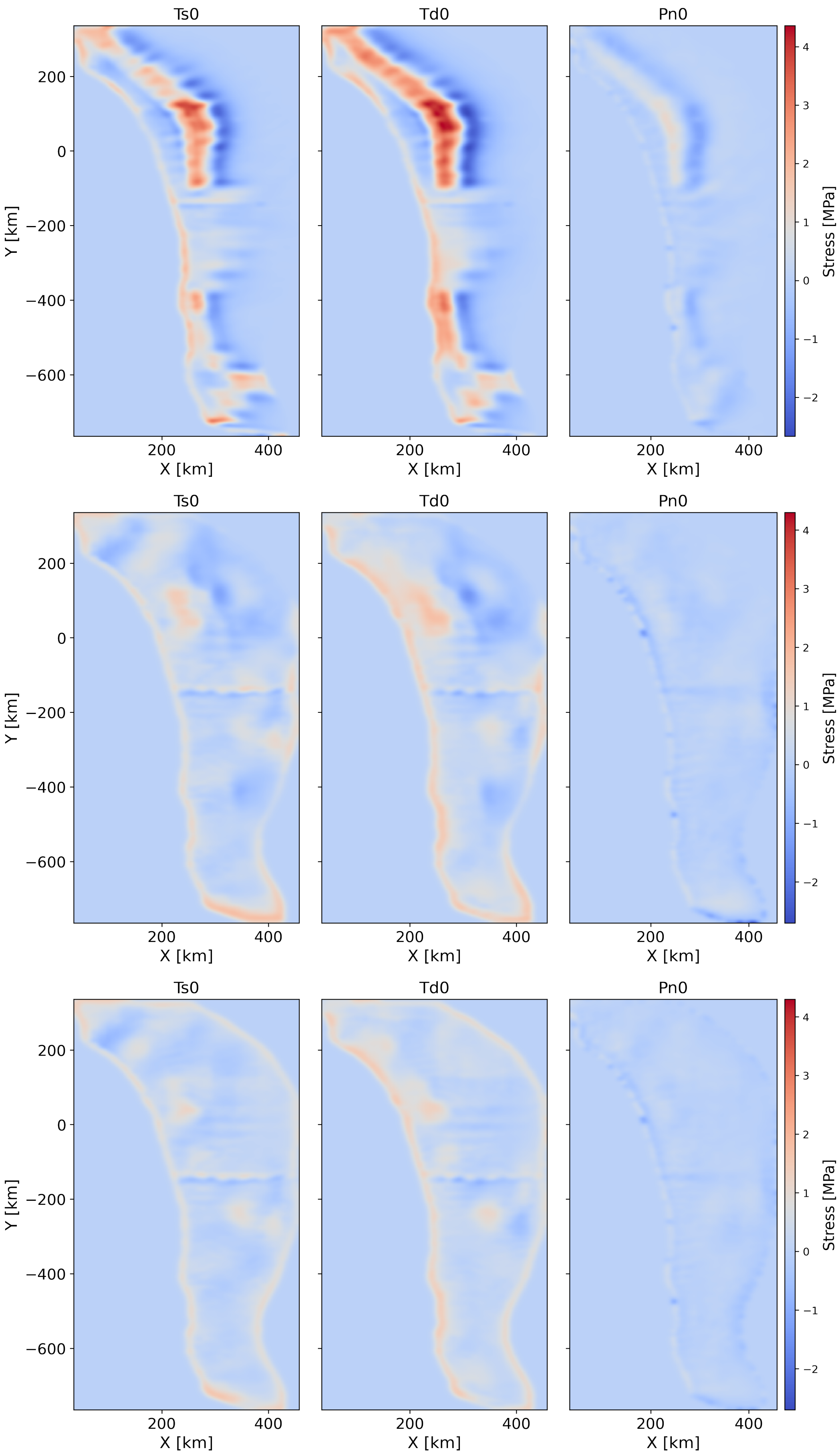

Figure S11: Example of stress changes from the dynamic relaxation simulation corresponding to a low rigidity and a very high P_f ratio ($\gamma = 0.97$): the shear stress changes in the strike ($\Delta\tau_{s0}$; left column) and dip ($\Delta\tau_{d0}$; middle column) directions, as well as the changes in the normal stresses (Δp_{n0}; right column) without tapering negative values. For the Gaussian SDM (upper panel), for the shallow-coupled 30 SDM with negative shear stress rate tapered up to a depth of 30 km (middle panel), and for the shallow-coupled 80 SDM with negative shear stress rate tapered up to a depth of 80 km (lower panel).

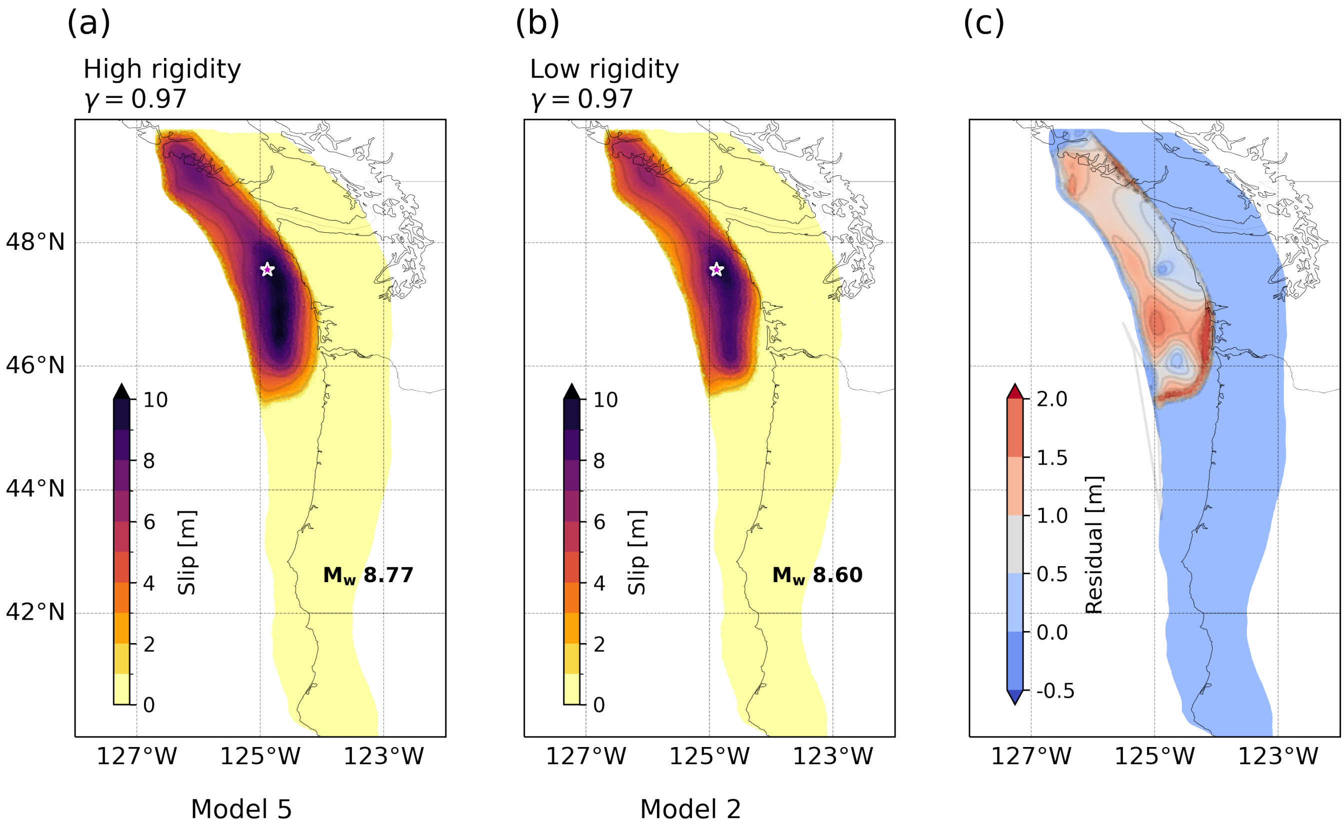

Figure S12: Comparison of modeled slip for (a) high rigidity (model 5) and (b) low rigidity (model 2) scenarios using a Gaussian SDM, and very high P_f ratio ($\gamma = 0.97$) with (c) the slip difference between the high rigidity model 5 and the low rigidity model 3 showing the combined effect of using high rigidity over the low rigidity in our simulations. The magenta star denotes the hypocenter where rupture is initiated (hypocenter).

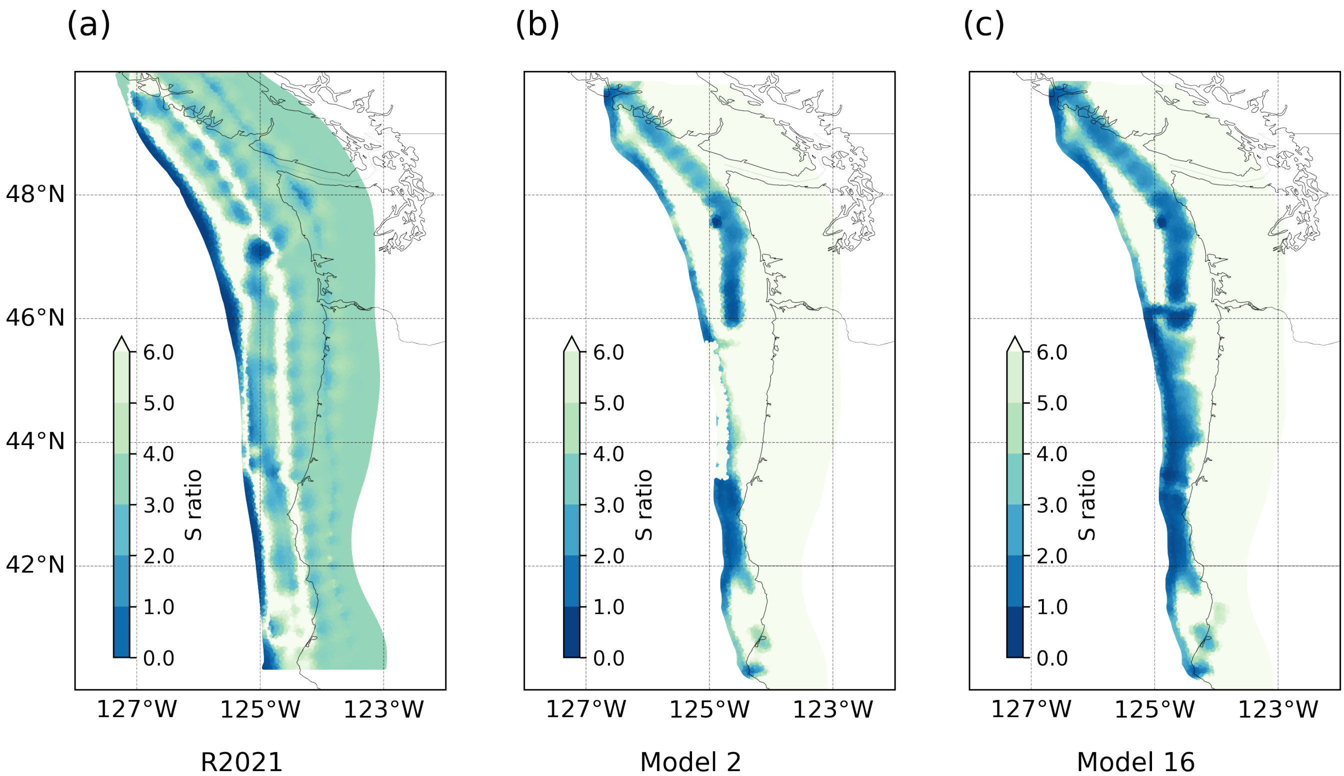

Figure S13: Comparison of the S ratio in (a) a margin-wide rupture simulation from Ramos et al. (2021) (R2021) and our study: (b) partial rupture dynamic simulation (model 2) and (c) margin-wide rupture (model 16). All models use the Gaussian SDM. Models 2 and R2021 use the same scaling factors (SF) to compute the slip deficit. Model 16 uses an elevated SF at central CSZ (latitude 43.2 to 46°N).

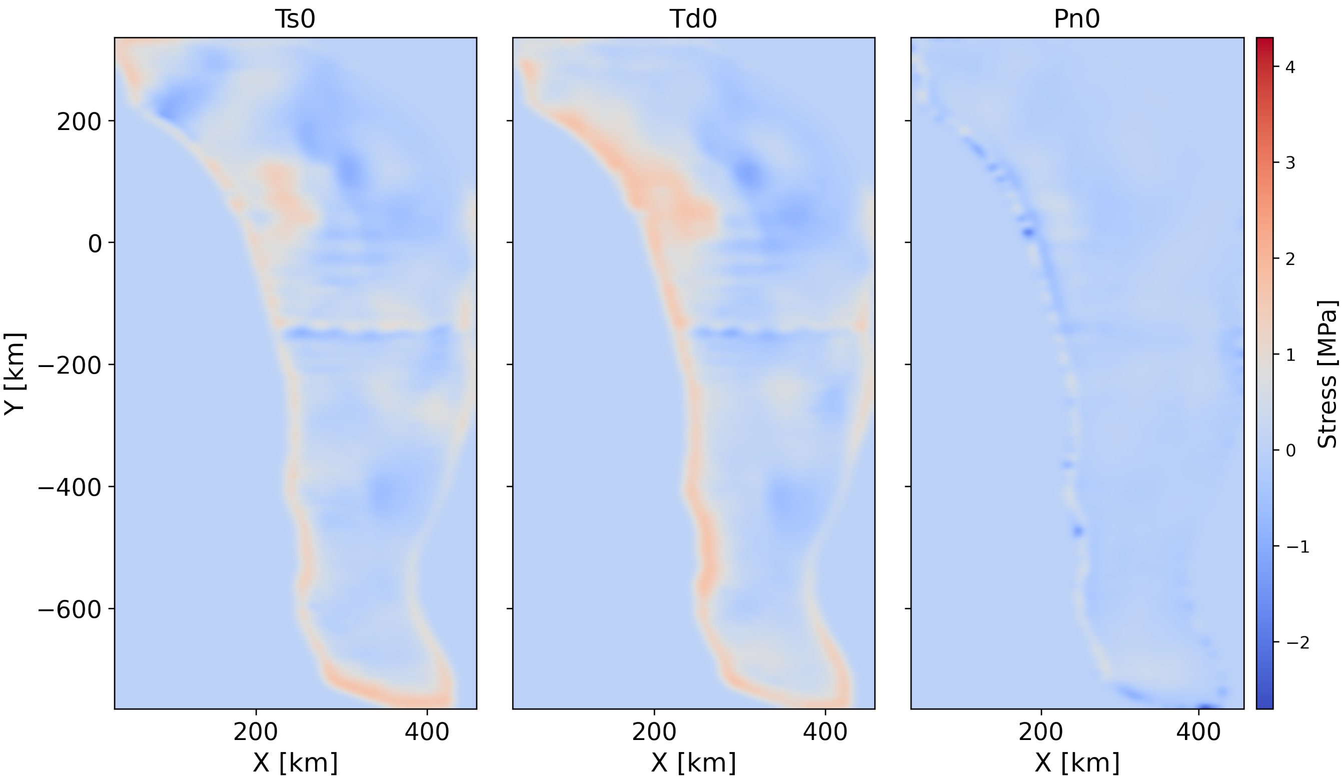

Figure S14: Stress changes from the dynamic relaxation simulation without tapering negative values for the shallow-coupled 30 SDM with negative shear stress rate tapered to be non-negative up to a depth of 30 km and a constant rigidity of 32 GPa. The shear stress changes in the strike ($\Delta\tau_{s0}$; left column) and dip ($\Delta\tau_{d0}$; middle column) directions, as well as the changes in the normal stresses (Δp_{n0}; right column) without tapering negative values.

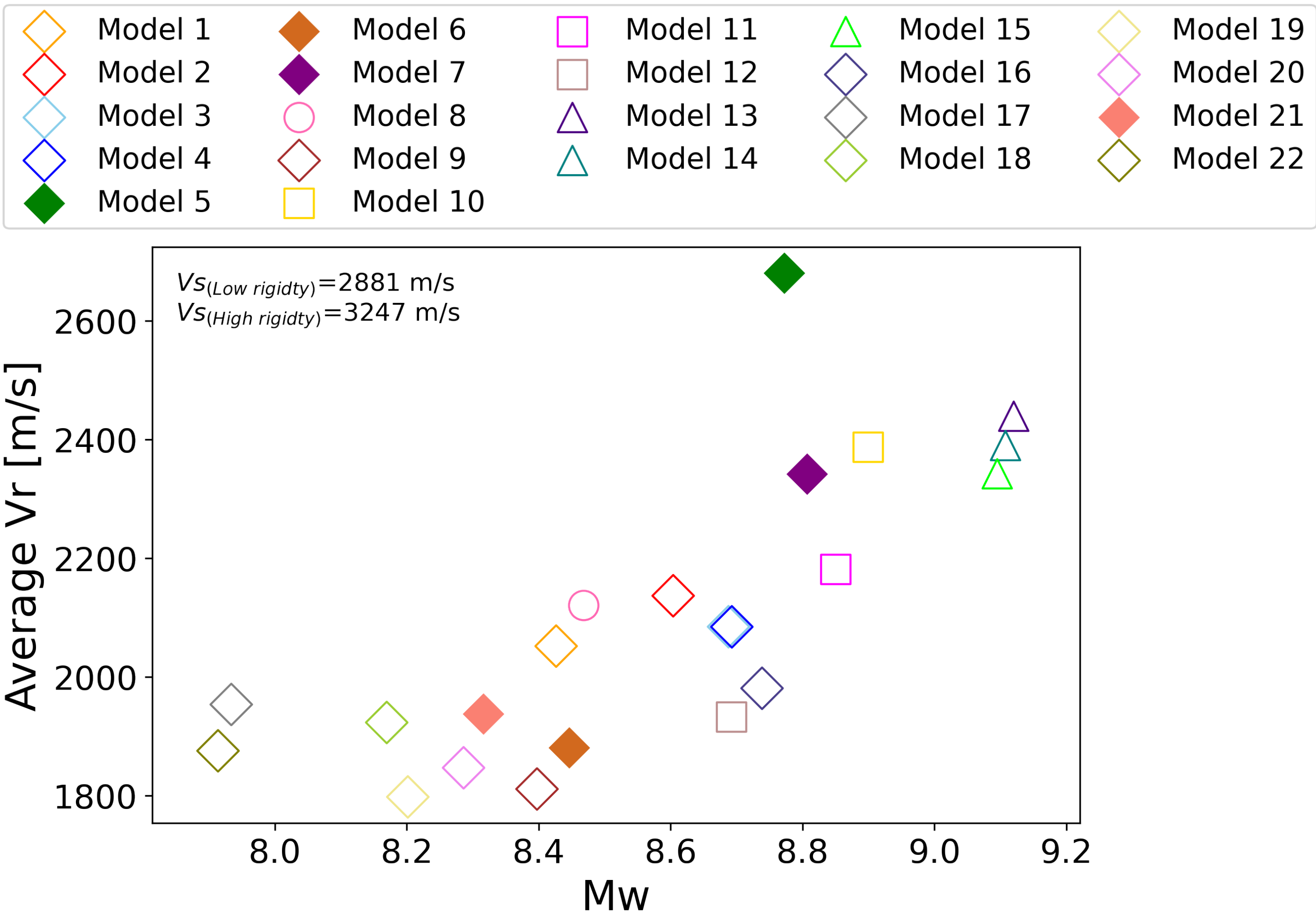

Figure S15: Average rupture velocity V_r for each of the 22 dynamic rupture scenarios and the respective moment magnitude $\mathrm{M_w}$. V_r remains subshear for all scenarios relative to the lowest S-wave speed in the seismogenic zone, i.e.,V_r>2881 m/s for the low rigidity and V_r>3247 m/s for the high rigidity dynamic rupture simulations. The various shapes and fillings represent different states of the P_f ratio and rigidity. Diamonds denote a very high P_f ratio ($\gamma = 0.96 - 0.97$), squares represent a high P_f ratio ($\gamma = 0.85 - 0.91$), and triangles represent a moderate-high P_f ratio ($\gamma = 0.65 - 0.71$). Model 8 (mixed P_f ratio) is represented by a circle. Empty markers indicate a scenario with low rigidity, while filled markers indicate scenarios with high rigidity (models 5, 7) or constant rigidity (models 6, 21).

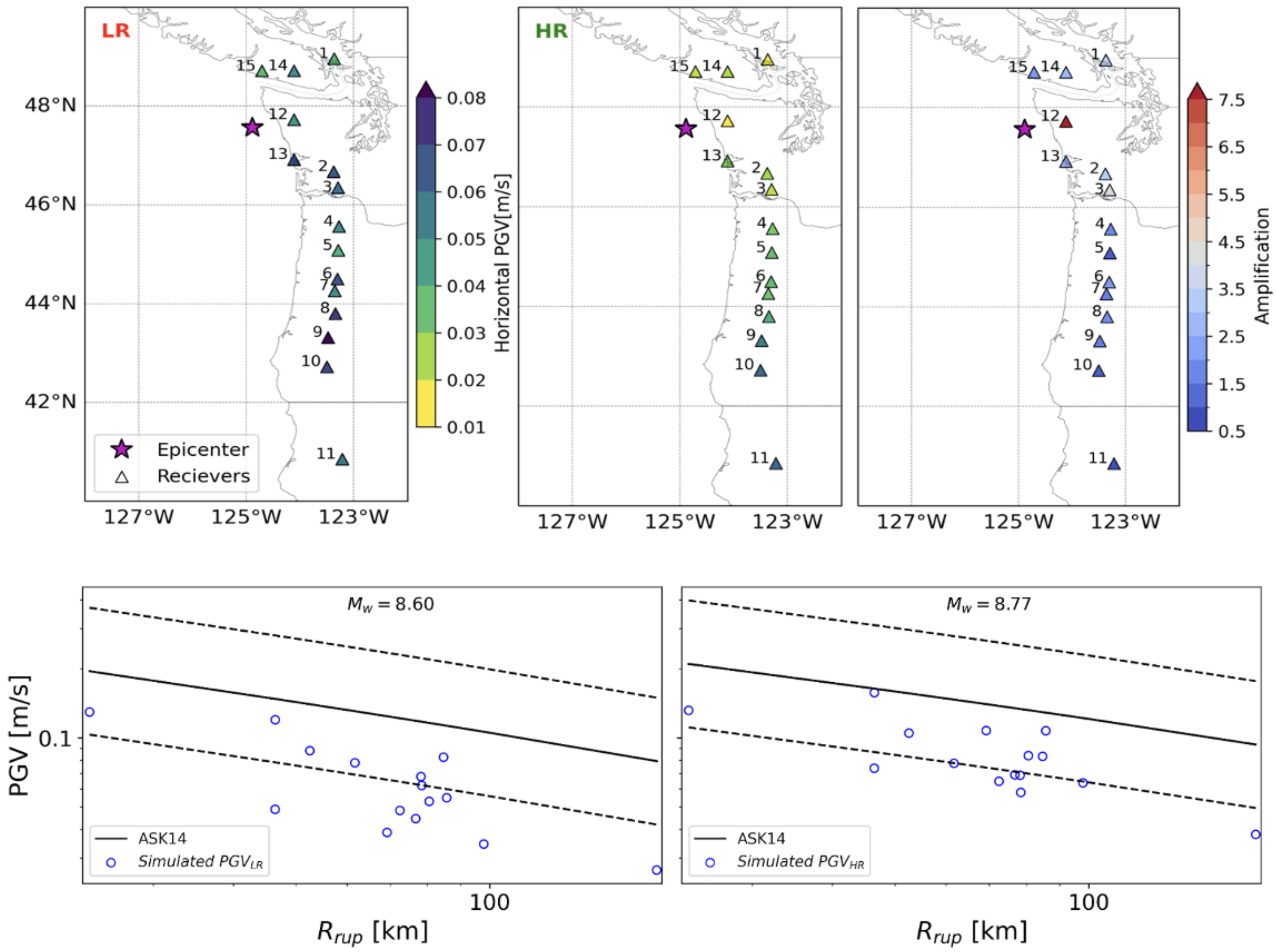

Figure S16: (Top) Simulated horizontal Peak ground velocities (PGVs) for the low rigidity model 2 (LR; left) and high rigidity model 5 (HR; middle) scenarios under the high pore fluid pressure assumption ($\gamma = 0.97$). (right) PGV amplification factors of the LR/ HR scenarios. (Bottom) PGV attenuation relationship of the respective models compared with the ASK14 ground motion prediction equation (Abrahamson et al., 2014)